JOURNAL OF SOLID STATE CHEMISTRY **124,** 220–223 (1996)
ARTICLE NO. 0229

Crystal Structure and Magnetic Properties of $(Mg_{6-x}Li_x)MnO_8$

Hideki Taguchi,[1] Akiko Ohta, and Mahiko Nagao

Research Laboratory for Surface Science, Faculty of Science, Okayama University, Okayama 700, Japan

Hiroyasu Kido

Osaka Municipal Technical Institute, Jyoto-Ku, Osaka 536, Japan

and

Hisanori Ando and Kenji Tabata

Research Institute of Innovation Technology for the Earth (RITE), Kizugawadai, Kizu-cho, Soraku-gun, Kyoto 619-02, Japan

Received January 2, 1996; in revised form March 12, 1996; accepted March 21, 1996

Murdochite-type $(Mg_{6-x}Li_x)MnO_8$ $(0.0 \leq x \leq 0.3)$ was synthesized at 973 K in a flow of pure oxygen gas using a solid state reaction. The cell constants, the (Mg, Li)–O(1) distance, and the Mn–O(1) distance monotonously decrease with increasing x. The variation of the effective magnetic moment (μ_{eff}) calculated from the magnetic measurement indicates that both the Mn^{4+} and the Mn^{5+} ions coexist in $(Mg_{6-x}Li_x)MnO_8$ $(0.0 \leq x \leq 0.2)$. The binding energies of the Mg $2s_{1/2}$, Li $1s_{1/2}$, Mn $2p_{3/2}$, and O $1s_{1/2}$ levels of $(Mg_{6-x}Li_x)MnO_8$ were determined by X-ray photoelectron spectroscopy (XPS), and they are independent of the composition. © 1996 Academic Press, Inc.

INTRODUCTION

Mg_6MnO_8 has the cubic murdochite-type structure with space group *Fm*3*m* (1, 2). Mg_6MnO_8 is considered to be derived from the rock-salt structure of MgO by the replacement of one-eighth of the Mg^{2+} ions with the Mn^{4+} ions and one-eighth with vacancies. The Mn^{4+} ions and vacancies occupy (1 1 1) alternate lattice layers and are ordered within the layers. Both the Mg^{2+} and the Mn^{4+} ions are octahedrally coordinated by six oxygen ions (1).

Porta and Valigi reported that the cell constant of Mg_6MnO_8 is 0.8381 ± 0.0002 nm (2). Mg_6MnO_8 has a weak antiferromagnetic interaction with $T_\theta = -20 \pm 5$ K, and μ_{eff} in the paramagnetic region is 3.94 ± 0.08 B.M. Mg_6MnO_8 is generally synthesized at high temperature (over 1173 K) in the flow of oxygen using a solid state reaction. Although the molar ratio of Mg/Mn in the starting materials was stoichiometric (6/1), the X-ray diffraction (XRD) pattern shows that the sample fired at high temperature is a mixture of Mg_6MnO_8 and MgO (1, 2). Recently, Taguchi and Nagao synthesized Mg_6MnO_8 from the stoichiometric molar ratio of Mg/Mn by using a sol–gel process (3).

Taguchi *et al.* synthesized $(Mg_{6-x}Al_x)MnO_8$ $(0 \leq x \leq 0.3)$ at low temperature using the solid state reaction (4). $(Mg_{6-x}Al_x)MnO_8$ has a mixed valence of the Mn^{3+} and the Mn^{4+} ions. The cell constants monotonously decrease with increasing x. From the results of the magnetic moment, both low-spin and high-spin states of the Mn^{3+} ions coexist. The binding energy of Mn $2p_{3/2}$ determined from x-ray photoelectron spectroscopy (XPS) measurement is independent of the composition. The full width at half maximum (FWHM) of the Mn $2p_{3/2}$ peak increases with increasing x. The presence of both low-spin and high-spin states of the Mn^{3+} ions causes an increase of the FWHM of the Mn $2p_{3/2}$ peak.

In the present study, we tried to synthesize murdochite-type $(Mg_{6-x}Li_x)MnO_8$ at low temperature using the solid state reaction. As the valence of the Li ion is 1+, both the Mn^{4+} and the Mn^{5+} ions must coexist in $(Mg_{6-x}Li_x)MnO_8$. We refined the structure refinement by Rietveld analysis, and made clear the electron configuration of both the Mn^{4+} and the Mn^{5+} ions.

EXPERIMENTAL

$(Mg_{6-x}Li_x)MnO_8$ $(0.0 \leq x \leq 0.3)$ was prepared using the solid state reaction. Powders of $Mg(CH_3COO)_2 \cdot 4H_2O$, $Li(CH_3COO) \cdot 2H_2O$, and $Mn(CH_3COO)_2 \cdot 4H_2O$ were weighted in the desired proportions and milled with acetone. After the mixed powders were dried, they were cal-

---

[1] To whom correspondence should be addressed.

0022-4596/96 $18.00

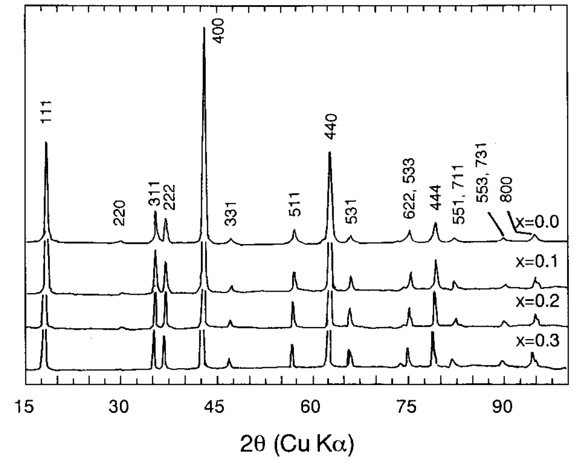

FIG. 1. X-ray powder diffraction patterns for $(Mg_{6-x}Li_x)MnO_8$.

cined at 673 K for 3 hr in a flow of pure oxygen gas. Then they were fired at 973 K for 6 hr in the flow of pure oxygen gas.

The phases of the samples were identified by X-ray powder diffractometer (XRD) with monochromatic Cu*Kα* radiation. The cell constants of the samples were determined from high-angle reflections. XRD data was collected by step scanning over an angular range $15° \leq 2\theta \leq 100°$ in increments of 0.02° (2θ). The structure refinement was carried out by Rietveld analysis of the X-ray powder diffraction data with the "RIETAN" program written by Izumi (5).

The magnetic susceptibility of the samples was measured by a magnetic torsion balance in the temperature range from 80 to 600 K. XPS measurement was carried out for the Mg 2*s*, Li 1*s*, Mn 2*p*, and O 1*s* levels of the samples using Mg*Kα* radiation at room temperature. The energy calibration was made against the C 1*s* peak from the usual contamination.

RESULTS AND DISCUSSION

XRD patterns of $(Mg_{6-x}Li_x)MnO_8 (0.0 \leq x \leq 0.3)$ were completely indexed as the cubic murdochite-type structure. Figure 1 shows the XRD patterns of $(Mg_{6-x}Li_x)MnO_8$ $(0.0 \leq x \leq 0.3)$. As $(Mg_{6-x}Li_x)MnO_8$ was synthesized below 973 K, we could not find MgO at all. In the range $x > 0.3$, the sample had both murdochite-type oxide peaks and extra peaks. The cell constants of $(Mg_{6-x}Li_x)MnO_8$ $(0.0 \leq x \leq 0.3)$ are shown in Table 1, and slightly decrease with increasing x. The cell constant of Mg_6MnO_8 is 0.83818 ± 0.0004 nm, which is equal to the value reported by Porta *et al.* (2). Since the structure of $(Mg_{6-x}Li_x)MnO_8$ is derived from the rock-salt structure, the coordination number (CN) of the Mg^{2+}, Li^+, Mn^{4+}, and Mn^{5+} ions is 6. The ionic radii of the Mg^{2+}, Li^+, Mn^{4+}, and Mn^{5+} ions are 0.072, 0.074, 0.053, and 0.045 nm, respectively (6, 7). The rate of increase for the ionic radius of $(Mg_{6-x}Li_x)MnO_8$ is calculated as follows. In this calculation, we assume that the MnO_6 octahedron in $(Mg_{6-x}Li_x)MnO_8$ has no distortion. Equations [1] and [2] are for the Mg site and for the Mn site, respectively:

$$(r_{\mathrm{Li}^{+}} - r_{\mathrm{Mg}^{2+}})/r_{\mathrm{Mg}^{2+}} = 2.8\% \qquad [1]$$

$$(r_{\mathrm{Mn}^{5+}} - r_{\mathrm{Mn}^{4+}})/r_{\mathrm{Mn}^{4+}} = -8.0\%. \qquad [2]$$

In these equations, r is the ionic radius. The rate of increase for the ionic radius of the Mn site is negative, and the absolute value for the Mn site is larger than that for the Mg site. From these results, the monotonic decrease of the cell constants is explained by the difference in the rate of increase for the ionic radii of the Mg site and the Mn site.

We carried out the structure refinement of $(Mg_{6-x}Li_x)MnO_8$ $(0.0 \leq x \leq 0.3)$ by Rietveld analysis of XRD data. The space group of Mg_6MnO_8 is *Fm3m* (1, 2). Therefore, it can be concluded that $(Mg_{6-x}Li_x)MnO_8$ has the same structure with space group *Fm3m*. Isotropic thermal parameters (B) for the Mg, Li, Mn, O(1), and O(2) ions were refined assuming that they had the same values. Refined

TABLE 1
Refined Structure Parameters for $(Mg_{6-x}Li_x)MnO_8$

Atom	Position	*x*	*y*	*z*	*B*
$x = 0.0$ $a = 0.83818(4)$ nm					
$R_{WP} = 14.29\%$		$R_P = 9.63\%$	$R_I = 3.45\%$	$R_F = 3.53\%$	
Mg	24(*d*)	0	0.25	0.25	0.005(2)
Mn	4(*a*)	0	0	0	0.005(2)
O(1)	8(*c*)	0.25	0.25	0.25	0.005(2)
O(2)	24(*e*)	0.230(2)	0	0	0.005(2)
$x = 0.1$ $a = 0.83781(2)$ nm					
$R_{WP} = 12.36\%$		$R_P = 8.70\%$	$R_I = 2.09\%$	$R_F = 1.99\%$	
Mg, Li	24(*d*)	0	0.25	0.25	0.006(2)
Mn	4(*a*)	0	0	0	0.006(2)
O(1)	8(*c*)	0.25	0.25	0.25	0.006(2)
O(2)	24(*e*)	0.228(2)	0	0	0.006(2)
$x = 0.2$ $a = 0.83774(1)$ nm					
$R_{WP} = 13.10\%$		$R_P = 8.96\%$	$R_I = 1.96\%$	$R_F = 2.27\%$	
Mg, Li	24(*d*)	0	0.25	0.25	0.006(2)
Mn	4(*a*)	0	0	0	0.006(2)
O(1)	8(*c*)	0.25	0.25	0.25	0.006(2)
O(2)	24(*e*)	0.228(2)	0	0	0.006(2)
$x = 0.3$ $a = 0.83748(1)$ nm					
$R_{WP} = 14.79\%$		$R_P = 10.61\%$	$R_I = 2.46\%$	$R_F = 2.42\%$	
Mg, Li	24(*d*)	0	0.25	0.25	0.006(2)
Mn	4(*a*)	0	0	0	0.006(2)
O(1)	8(*c*)	0.25	0.25	0.25	0.006(2)
O(2)	24(*e*)	0.229(2)	0	0	0.006(2)

TABLE 2
(Mg, Li)–O and Mn–O Distances (nm) for $(Mg_{6-x}Li_x)MnO_8$

x	(Mg, Li)–O(1)	(Mg, Li)–O(2)	Mn–O(1)	Mn–O(2)
0.0	0.20955	0.2102(1)	0.20955	0.1925(16)
0.1	0.20945	0.2102(1)	0.20945	0.1912(14)
0.2	0.20943	0.2102(1)	0.20943	0.1912(14)
0.3	0.20937	0.2101(1)	0.20937	0.1918(17)

structure parameters and residuals, weighted pattern R factor (R_{WP}), pattern R factor (R_P), integrated R factor (R_I), and structure factor (R_F) are listed in Table 1. The final R_F of all samples was less than 3.53%. The present result suggests that the structure model for $(Mg_{6-x}Li_x)MnO_8$ is good.

Table 2 shows the (Mg, Li)–O and the Mn–O distances of $(Mg_{6-x}Li_x)MnO_8$ calculated from the refined structure parameters. In the murdochite-type structure, the (Mg, Li)–O(1) distance is equal to the Mn–O(1) distance. Both the (Mg, Li)–O(1) and the Mn–O(1) distances decrease with increasing x. On the other hand, both the (Mg, Li)–O(2) and the Mn–O(2) distances are independent of the composition. There are two types of the MgO_6 octahedra (A and B) in $(Mg_{6-x}Li_x)MnO_8$. The MgO_6 octahedron (A) has four O(1) and two O(2) ions, and the MgO_6 octahedron (B) has two O(1) and four O(2) ions. The MgO_6 octahedra (A) and (B) share edges with each other. Since the Mn–O(1) distance is longer than the Mn–O(2) distance, it is obvious that the MnO_6 octahedron has a distortion.

The magnetic susceptibility (χ) of $(Mg_{6-x}Li_x)MnO_8$ ($0.0 \leq x \leq 0.3$) was measured in the temperature range from 80 to 600 K. Figure 2 shows the temperature dependence of the inverse magnetic susceptibility ($1/\chi$) for $(Mg_{5.9}Li_{0.1})MnO_8$ ($x = 0.1$). The $1/\chi$–T curves for $(Mg_{6-x}Li_x)MnO_8$ ($0.0 \leq x \leq 0.3$) are linear and follow the Curie–Weiss law above 300 K. $(Mg_{6-x}Li_x)MnO_8$ is paramagnetic with paramagnetic Curie temperature (T_θ) = 6.9 K for $x = 0.0$, 14.5 K for $x = 0.1$, 18.7 K for $x = 0.2$, and 33.1 K for $x = 0.3$, respectively. We calculated the effective magnetic moment (μ_{eff}) from the linear portion of the $1/\chi$–T curves. Figure 3 shows the relationship between the observed μ_{eff} and x. In Fig. 3, the open circles indicate the observed μ_{eff}. The observed μ_{eff} for $x = 0.0$ is 3.87 ± 0.05 B.M., and this value is nearly equal to the value reported by Porter and Valigi (2). The observed μ_{eff} slightly decreases with increasing x. The line in Fig. 3 indicates the theoretical μ_{eff} that was calculated on the assumption of the coexistence of the Mn^{4+} ion with the $(d\varepsilon)^3(d\gamma)^0$ and the Mn^{5+} ion with the $(d\varepsilon)^2(d\gamma)^0$. As seen in Fig. 3, the observed μ_{eff} in the range $0.0 \leq x \leq 0.2$ agree with the theoretical μ_{eff}. On the other hand, although $(Mg_{5.7}Li_{0.3})MnO_8$ ($x = 0.3$) has the murdochite-type structure, the observed μ_{eff} is 3.72 ± 0.05 B.M. and larger by ca. 0.13 B.M. than the theoretical μ_{eff}. These results indicate that both the Mn^{4+} and the Mn^{5+} ions coexist in $(Mg_{6-x}Li_x)MnO_8$ ($0.0 \leq x \leq 0.2$) and the ratio of Mn^{5+}/Mn^{4+} increases linearly with x.

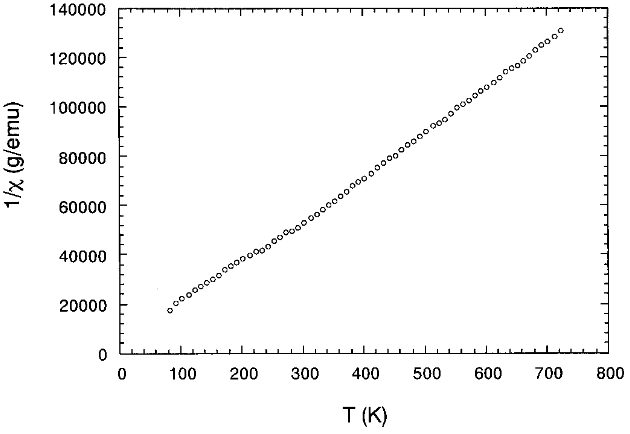

FIG. 2. Inverse magnetic susceptibility ($1/\chi$) vs temperature (T) for $(Mg_{5.9}Li_{0.1})MnO_8$ ($x = 0.1$).

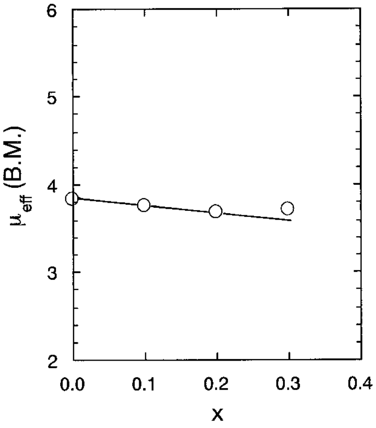

FIG. 3. Effective magnetic moment (μ_{eff}) vs composition (x) for the system $(Mg_{6-x}Li_x)MnO_8$. The line indicates the theoretical values calculated on the assumption of the coexistence of the Mn^{4+} ion with $(d\varepsilon)^3(d\gamma)^0$ and the Mn^{5+} ion with $(d\varepsilon)^2(d\gamma)^0$.

We measured the XPS spectra of the Mg $2s_{1/2}$, Li $1s_{1/2}$, Mn $2p_{3/2}$, and O $1s_{1/2}$ levels of $(Mg_{6-x}Li_x)MnO_8$. The binding energies of Mg $2s_{1/2}$, Li $1s_{1/2}$, Mn $2p_{3/2}$, and O $1s_{1/2}$ are independent of the composition; 50.1 ± 0.1 eV for Mg $2s_{1/2}$, 53.7 ± 0.7 eV for Li $1s_{1/2}$, 643.7 ± 0.2 eV for Mn $2p_{3/2}$ and 530.6 ± 0.1 eV for O $1s_{1/2}$. The XPS spectrum of the Mn $2p_{3/2}$ level is broad and asymmetric toward the high binding energy site as shown in Fig. 4. Kowalczyk *et al.* reported that the broad and asymmetric Mn $2p_{3/2}$ peak in MnF_2 is due to the multiple splitting (8). The binding energies of Mg $2s_{1/2}$, Al $2s_{1/2}$, Mn $2p_{3/2}$, and O $1s_{1/2}$ in

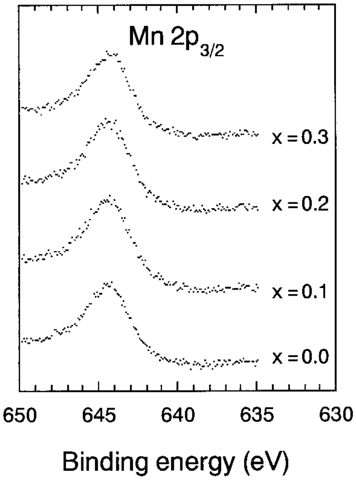

FIG. 4. XPS spectra of the Mn $2p_{3/2}$ level of $(Mg_{6-x}Li_x)MnO_8$.

murdochite-type $(Mg_{6-x}Li_x)MnO_8$ are also independent of the composition (4). Taguchi *et al.* reported the binding energy of Nd $4d_{3/2}$, Ca $2p_{3/2}$, Mn $2p_{3/2}$, and O $1s_{1/2}$ in perovskite-type $(Nd_{1-x}Ca_x)MnO_{2.99}$ (9). The binding energies of Nd $4d_{3/2}$, Ca $2p_{3/2}$, and O $1s_{1/2}$ decrease with increasing x. On the other hand, the binding energy of Mn $2p_{3/2}$ is independent of the composition. The variation of the binding energy is due to the partial ionic character of Nd and Ca. The decrease of O $1s_{1/2}$ is due to an increase of the valence in the Mn ion. In the present system, the ionic character of the cation in $(Mg_{6-x}Li_x)MnO_8$ is not strongly affected by the substitution of the Li^+ ion for the Mg^{2+} ion.

There are two types of chemical bonding in $(Mg_{6-x}Li_x)MnO_8$. One is Mg^{2+}–O^{2-}–(Mg^{2+} or Li^+) and the other is Mg^{2+}–O^{2-}–(Mn^{4+} or Mn^{5+})–O^{2-}–(Mg^{2+} or Li^+). Since the occupation rate of the Li^+ ion at the Mg^{2+} ion sites is less 5.3%, the binding energy of Mg $2s_{1/2}$ in the chemical bonding of Mg^{2+}–O^{2-}–(Mg^{2+} or Li^+) is not strongly affected by the Li^+ ion. Carver *et al.* reported that the binding energy of Mn $2p_{3/2}$ for MnI_2, $MnBr_2$, $MnCl_2$, MnF_2, MnS, and MnO is 642.1, 642.2, 642.1, 642.8, 640.5, and 641.7 eV, respectively (10). These results suggest that the binding energy of Mn $2p_{3/2}$ for Mn–X_2 or Mn–X (X = halogen or chalcogen) increases with increasing the electronegativity of A. On the other hand, the binding energy of Mn $2p_{3/2}$ decreases with decreasing the valence of the Mn ion; the binding energy of Mn $2p_{3/2}$ for $Mn^{4+}O_2$, $Mn^{3+}{}_2O_3$, and $Mn^{2+}O$ is 642.4, 641.8, and 641.7 eV, respectively (10). The electronegativity of Li, Mg, Mn^{3+}, and Mn^{7+} is 1.0, 1.2, 1.5, and 2.3, respectively (11). From these values, it is obvious that the electronegativity of the Mn ion increases with increasing the valence of the Mn ion. Therefore, the electronegativity of the Mn^{5+} ion is larger than that of the Mn^{4+} ion. Now, we consider the chemical bonding of (Mn^{4+} or Mn^{5+})–O^{2-}. The binding energy of Mn $2p_{3/2}$ decreases with increasing the valence of the Mn ion. On the other hand, the binding energy of Mn $2p_{3/2}$ increases with decreasing the electronegativity from the Mn^{4+} ion to the Mn^{5+} ion. Both the increase and the decrease of the binding energy of Mn $2p_{3/2}$ occur simultaneously. Consequently, we could not observe the variation of the chemical shift of Mn $2p_{3/2}$ with the composition.

CONCLUSION

The structure refinement of $(Mg_{6-x}Li_x)MnO_8$ ($0.0 \leq x \leq 0.3$) indicates that the cell constants, the (Mg, Li)–O(1) distance, and the Mn–O(1) distance monotonically decrease with increasing x. From the results of the magnetic measurement, the $1/\chi$–T curve obeys the Curie–Weiss law above 300 K. The variation of μ_{eff} indicates that the ratio of Mn^{5+}/Mn^{4+} linearly increases with x in the range $0.0 \leq x \leq 0.2$. The binding energies of the Mg $2s_{1/2}$, Li $1s_{1/2}$, Mn $2p_{3/2}$, and O $1s_{1/2}$ levels of $(Mg_{6-x}Li_x)MnO_8$ are independent of the composition. This independence is explained by the decrease of the binding energy due to the increase of the valence of the Mn ion and the increase of the electronegativity of the Mn ion.

ACKNOWLEDGMENT

This work was partly supported by NEDO (New Energy and Industrial Technology Development Organization, Japan).

REFERENCES

1. J. S. Kasper and J. S. Prener, *Acta. Crystallogr.* **7,** 246 (1954).
2. P. Porta and M. Valigi, *J. Solid State Chem.* **6,** 344 (1973).
3. H. Taguchi and M. Nagao, *J. Mater. Sci. Lett.* **10,** 658 (1991).
4. H. Taguchi, A. Okamoto, M. Nagao, and H. Kido, *J. Solid State Chem.* **102,** 570 (1993).
5. F. Izumi, *Nippon Keshou GakKai-shi* **27,** 23 (1986). [in Japanese]
6. R. D. Shannon and R. D. Prewitt, *Acta Crystallogr. Sect. B* **25,** 925 (1969).
7. V. M. Tromel, *Acta Crystallogr. Sect. B* **39,** 664 (1983).
8. S. P. Kowalczyk, L. Ley, F. R. McFeely, and D. A. Shirley, *Phys. Rev. B* **11,** 1721 (1975).
9. H. Taguchi, M. Nagao, M. Shimada, Y. Takeda, and O. Yamamoto, *J. Solid State Chem.* **77,** 336 (1988).
10. J. C. Carver, G. K. Scheritzer, and T. A. Carlson, *J. Chem. Phys.* **57,** 973 (1972).
11. W. Gordy and J. O. Thomas, *J. Chem. Phys.* **24,** 439 (1956).